JACS
JOURNAL OF THE AMERICAN CHEMICAL SOCIETY

ARTICLE

pubs.acs.org/JACS

Valence-to-Core X-ray Emission Spectroscopy: A Sensitive Probe of the Nature of a Bound Ligand

Christopher J. Pollock and Serena DeBeer*

Department of Chemistry and Chemical Biology, Cornell University, Ithaca, New York 14853, United States

Supporting Information

ABSTRACT: The sensitivity of iron Kβ X-ray emission spectroscopy (XES) to the nature of the bound ligands (σ-donating, π-donating, and π-accepting) has been explored. A combination of experiment and theory has been employed, with a DFT approach being utilized to elucidate ligand effects on the spectra and to assign the spectral intensity mechanisms. Knowledge of the various contributions to the spectra allows for a deeper understanding of spectral features and demonstrates the sensitivity of this method to the identity of the interacting ligands. The potential of XES for identifying intermediate species in nonheme iron enzymes is highlighted.

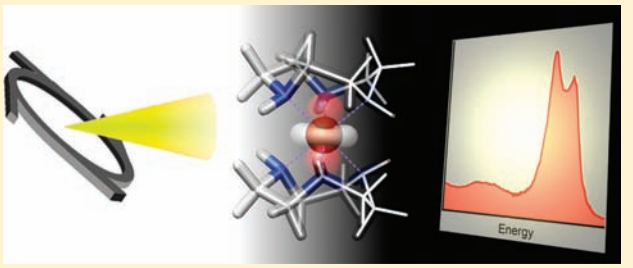

INTRODUCTION

Metalloenzymes containing iron are of critical importance to many biological processes, including hydrocarbon oxidation and nitrogen fixation.[1−4] Many of these reactions are of considerable interest on both laboratory and industrial scales, fueling investigation into these enzymes with the hope of mimicking their reactivities. Harnessing and replicating these reactivities requires detailed knowledge of the enzymes' geometric and electronic structures; to this end, crystallography and spectroscopy have shed much light onto many of these systems. Metal spin and oxidation states of resting enzymes and even many intermediates have been determined by electron paramagnetic resonance (EPR), X-ray absorption (XAS), X-ray magnetic circular dichroism (X-MCD), and Mössbauer, while structural information has been obtained from resonance Raman, extended X-ray absorption fine structure (EXAFS), and magnetic circular dichroism (MCD).[5−11]

Despite the insights from these tools, many questions about these metal centers and their ligand frameworks still remain, especially with respect to reactive intermediates. The oxygen binding mode in intermediate Q of methane monooxygenase[12] and the protonation state of the compound II intermediates in heme enzymes[8,13] provide two examples of enduring uncertainties. One reason for the persistence of these questions is the lack of spectroscopic techniques that readily probe the bound ligands. Of the techniques that are sensitive to ligand identity, EXAFS is unable to differentiate between C, N, and O scatterers, while EPR and vibrational analyses require isotope substitution, often a prohibitive challenge in a protein matrix. Perhaps the most sensitive well-established probe of ligand identity is photoemission spectroscopy, but here the requirement for ultrahigh vacuum conditions greatly limits the systems to which it may be applied.

Even if these aforementioned challenges could be overcome, it is still exceedingly difficult to probe beyond the atoms immediately bound to the metal. EXAFS, for example, could potentially differentiate between a bound water and a hydroxide ion based on bond length differences, but may not be able to discriminate a water from a carboxylate. While it is possible to investigate beyond the first coordination sphere with complex ENDOR, ESEEM, and NMR experiments, these all require the presence of sizable couplings, limiting their application.[14,15] The power to easily distinguish between ligands that provide similar coordination environments, such as water versus oxidized substrate, is of utmost importance in complex systems such as enzyme active sites, although to do so requires a currently unavailable means of probing the ligand electronic structure. Thus, the difficulties and limitations endemic to currently available methods warrant the development of new techniques capable of more thoroughly investigating the ligands around a metal center.

It is here, as a spectroscopic probe of the ligand environment, that Fe Kβ X-ray emission spectroscopy (XES) holds promise.[16,17] This technique involves ionizing a 1s core electron on Fe by incident high energy X-rays, followed by monitoring the emission of photons during electron decay to fill the 1s hole (Figure 1).[18] The features of chemical interest are the K$\beta_{1,3}$ emission, an electric dipole-allowed 3p−1s transition that is dominated by 3p−3d exchange correlation with a lesser 3p spin−orbit coupling component, and the Kβ''/K$\beta_{2,5}$ "valence-to-core" emissions, which stem from transitions from the filled ligand valence ns and np orbitals, respectively, to the Fe 1s core hole.[19] Fe Kβ XES has already been shown to be sensitive both toward metal spin and oxidation state, as well as ligand identity, hybridization, and

Received: January 19, 2011
Published: March 18, 2011

dx.doi.org/10.1021/ja200560z | J. Am. Chem. Soc. 2011, 133, 5594–5601

protonation.[16] Of particular interest is the valence-to-core region because these features represent transitions from filled orbitals that are dominantly ligand in nature. Despite the rich information content of this region, the exact mechanisms and selection rules underpinning intensities have yet to be fully understood.

Fortunately, Fe Kβ XES spectra can be modeled with excellent agreement to experiment by density functional theory (DFT), thus providing a means to gain further insight into these spectra. Figure 2 shows a comparison of the experimental XES data for $Fe(TACN)_2^{3+}$, $Fe(acac)_3$, and $Fe(CN)_6^{3-}$ (TACN = 1,4,7-triazacyclononane, acac = acetylacetonate) and the corresponding calculated spectra.[16] Analysis of the dominant contributions by DFT demonstrated that the valence-to-core region of XES spectra is comprised primarily of contributions from the ligands. As shown in Figure 2, in the case of a pure σ-donating ligand (such as TACN), only a single feature in the XES K$\beta_{2,5}$ region is observed, while for the π-donating and π-accepting ligands, acac and CN^-, respectively, two features are observed. It thus seems intuitive that the nature of the ligand must influence the spectra, although a thorough investigation of ligand contributions has not been previously undertaken. For instance, contributions from the σ and π frameworks have not been established, nor are the intensity mechanisms fully understood. To exploit the potential of XES for investigating proteins, detailed knowledge of exactly why these features arise for π-donors and acceptors but not for σ-only donors, as well as more general knowledge about what governs intensity, is required.

The present study employs a DFT approach to investigate in detail the origins of the valence-to-core features and the mechanisms governing their intensity. As the iron valence-to-core spectra have been previously shown to be dominated by Fe np to Fe 1s transitions, we have undertaken a theoretical investigation from the perspective of both the metal emission and the ligand emission (Figure 3) to unambiguously understand the ligand contributions.[16] For first row elements, examining the Kα ligand (nitrogen or oxygen in the current investigation) emissions is critical because they provide a measure of the ligand electronic structure,[20,21] similar to photoemission spectroscopy, that can be correlated to the iron XES spectra, thus giving a more complete picture of how the ligand contributes to the experimental spectra. These studies form a foundation for establishing this technique as a selective probe of the ligand environment and determining the factors governing intensity. The 4p contributions of the metal to bonding orbitals are also discussed. Finally, the extension of these methods and the possibility for using valence-to-core XES for understanding metal substrate interactions in metalloprotein active sites is highlighted.

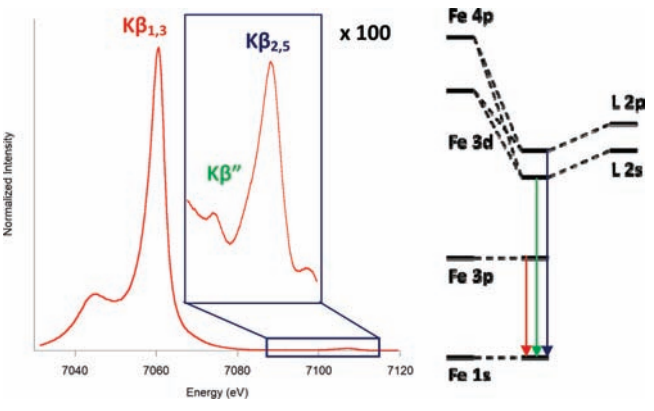

Figure 1. Fe Kβ XES spectrum of Fe_2O_3 with valence-to-core region enlarged roughly 100-fold. The simplified molecular orbital (MO) diagram on the right schematically depicts the origin of the features in the spectrum.

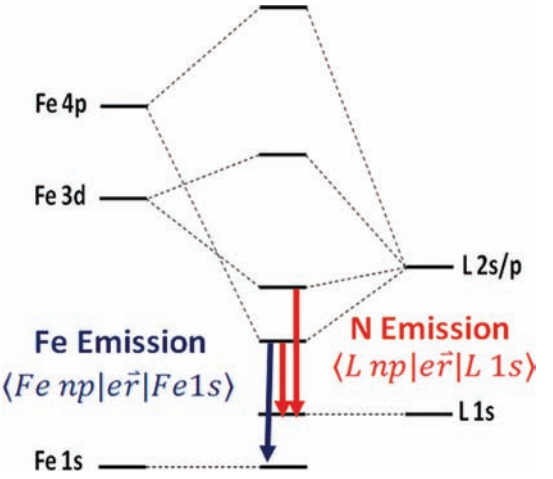

Figure 3. Schematic of the two types of transitions employed in this work: Fe np to Fe 1s (Fe Kβ valence-to-core XES, blue) and ligand 2p to ligand 1s (ligand Kα XES, red).

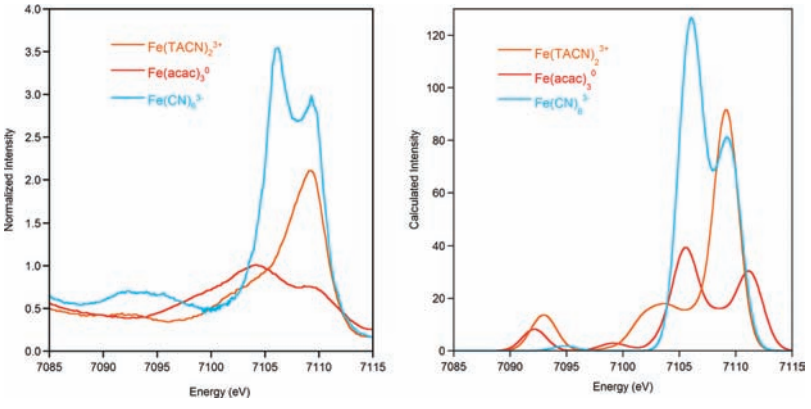

Figure 2. Comparison between experimental and DFT calculated valence-to-core Fe Kβ XES spectra for $Fe(TACN)_2^{3+}$, $Fe(acac)_3$, and $Fe(CN)_6^{3-}$. A 2.5 eV broadening and 182.5 eV energy shift have been applied to the calculated spectra.[16]

dx.doi.org/10.1021/ja200560z |J. Am. Chem. Soc. 2011, 133, 5594–5601

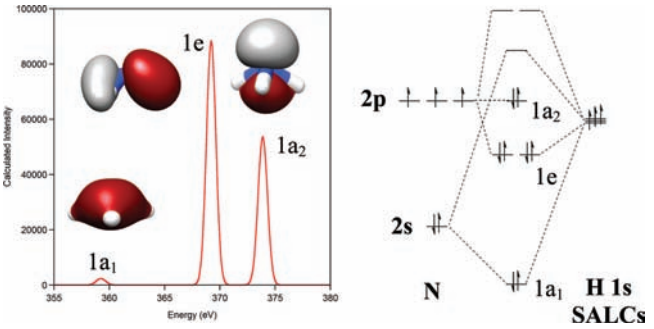

Figure 4. Comparison showing a nitrogen Kα XES spectrum of NH_3 (N 2p → N 1s transitions, left) with transitions labeled according to their symmetry from the NH_3 molecular orbital diagram (right).

CALCULATIONS

All calculations were performed using the ORCA quantum chemistry software package.[22] Nitrogen Kα and iron Kβ XES spectra were calculated on either optimized or idealized structures (specified in text) using the protocol described previously.[16] The BP86 functional[23,24] was utilized with the TZVP[25] basis set on all atoms excluding Fe, which had an expanded CP(PPP) basis set.[26] Solvation was modeled using the conductor-like screening model (COSMO)[27] in an infinite dielectric. Geometry optimizations were performed using the same level of theory. Constructs involving octahedral arrangements of ligands around point charges were obtained by first optimizing the corresponding ferric structure followed by subsequent replacement of the iron with a point charge; no further optimizations were carried out. Molecular orbitals were visualized using Chimera.[28] A 2.5 eV broadening was applied to all calculated iron emission spectra, and a 1 eV broadening was applied to all calculated ligand (N and O) emission spectra.

RESULTS AND ANALYSIS

Mechanisms Governing Spectral Intensity. Because the nature of the ligands bound to the metal was found to greatly impact XES spectra,[16] emphasis was placed on correlating the ligand electronic structure to the valence-to-core region of Fe XES spectra. For ease of analysis, a complex with only simple σ-donating ligands was considered first (ferric hexammine, $Fe(NH_3)_6^{3+}$). DFT calculations were performed using established computational methods (sample input file included in the Supporting Information) on free NH_3 without any metal present to establish the ligand's electronic structure. The structure was first optimized, and then a nitrogen XES spectrum was calculated using transitions from the valence N 2p orbitals to a N 1s hole (Kα emission), allowing the observation of the energetics of the NH_3 molecular orbitals (Figure 4). Clear transitions are observed from all expected valence molecular orbitals (MOs), and the relative energies obtained are in good agreement with previous photoelectron spectroscopic results.[29−31] Furthermore, the XES calculation was used to assess the relative contributions to the spectrum from electric dipole, magnetic dipole, and electric quadrupole mechanisms. Analysis of these transitions revealed they derived almost exclusively from electric dipole-allowed character (>99.5%), as would be expected for Kα emission.

Once the features of the free NH_3 emission spectrum were established, another level of complexity was added by arranging six ammonias into an octahedral geometry around a central point charge; this was equivalent to replacing the iron of $Fe(NH_3)_6^{3+}$ with a point charge, Q. The charge of Q was then varied

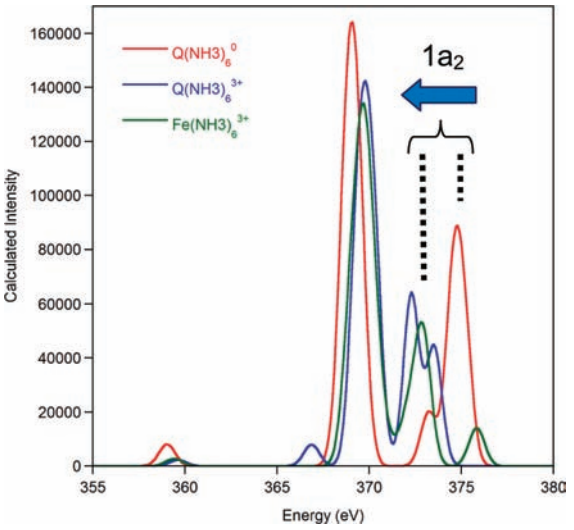

Figure 5. Nitrogen emission spectra from a construct of six ammonias around a central moiety, either a point charge of 0 or +3 or a ferric ion. Spectra are quite similar in energy and intensity of features, except for stabilization of the $1a_2$ lone pair by charge as indicated by arrow.

incrementally from 0 to +3, keeping the geometry of the ammonias constant, and nitrogen XES spectra were calculated for each of these charges (Supporting Information). The spectra remain similar to that from Figure 4, although, as expected, increasing the charge of Q resulted in increasing stabilization of the $1a_2$ lone pair orbital, up to roughly 3 eV, while the $1a_1$ and 1e N−H bonding orbitals were slightly destabilized (<0.7 eV). Slight additional splitting is also seen for the $1a_2$ feature resulting from the various phase combinations of the six lone pairs in octahedral symmetry ($a_{1\,g}$ vs e_g vs t_{1u}).

Using this same octahedral framework, the point charge was replaced by an Fe^{3+} ion, and the N emission was again analyzed (Figure 5). The spectrum thus obtained is remarkably similar, both in terms of energy and intensity of transitions, to that with only a Q^{3+} instead of Fe^{3+}, suggesting that an iron ion and a point charge are similar perturbations on the ligand orbitals.

The identification of the spectral features in the nitrogen Kα emission spectrum of $Fe(NH_3)_6^{3+}$ allows for direct comparison to the iron Kβ emission for the same compound by aligning the N 2s emission feature in both spectra (Figure 6). Excellent energetic agreement is seen for all features between the two spectra, providing further proof that iron valence-to-core Kβ XES spectra are dominated by ligand electronic structure. The relative intensities, however, differ markedly between the two cases. A factor of 1000 difference in intensity is expected between the Kα and $Kβ_{2,5}$ emission spectra (nitrogen and iron, respectively) due to the relative probabilities of each of these transitions,[19] with additional contributions possible due to differences in the intrinsic dipole moment of Fe and N.

Qualitatively, it can be seen that intensity is roughly modulated by the degree of overlap between the ligand and metal molecular orbitals; there is less overlap between the metal and the N 2s orbital as compared to the lone pair, and this is reflected in the relative intensities. Closer inspection of the transitions in the iron spectrum, however, reveals that all features with significant intensity derive from combinations of ammonia molecular orbitals possessing t_{1u} symmetry (notice the unresolved e_g lone pair feature at 6931 eV). Notably, this is the same symmetry as the iron p orbitals in octahedral geometry, implicating metal p

dx.doi.org/10.1021/ja200560z |J. Am. Chem. Soc. 2011, 133, 5594–5601

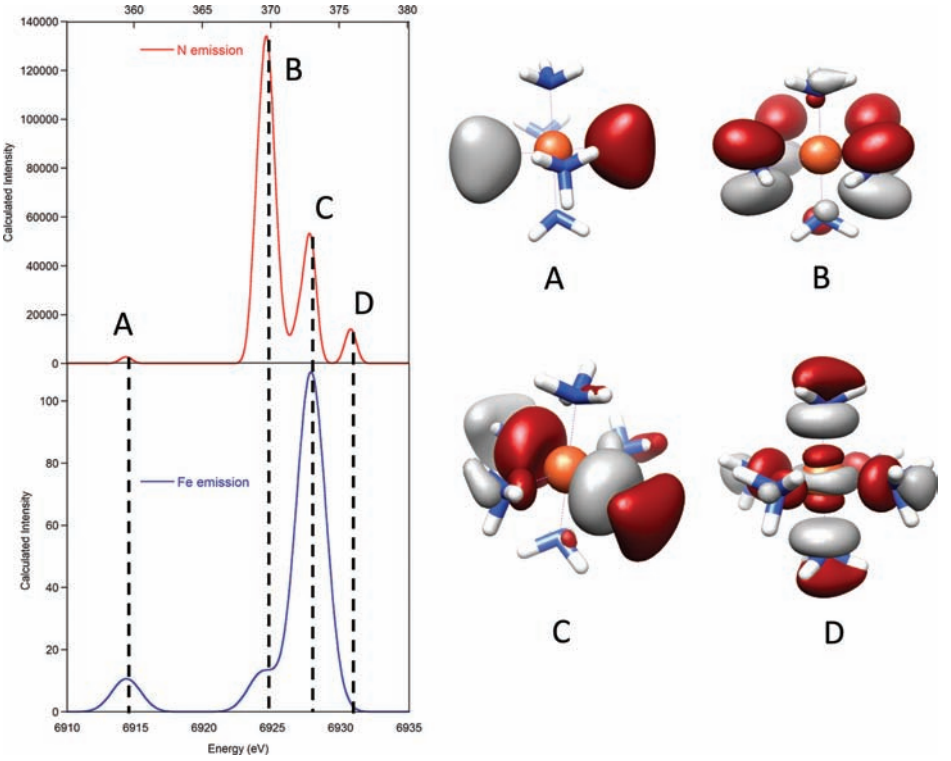

Figure 6. Comparison of N and Fe emission spectra from $Fe(NH_3)_6^{3+}$ showing intensity modulation from the perspective of iron. Representative MOs from each transition are plotted on the right.

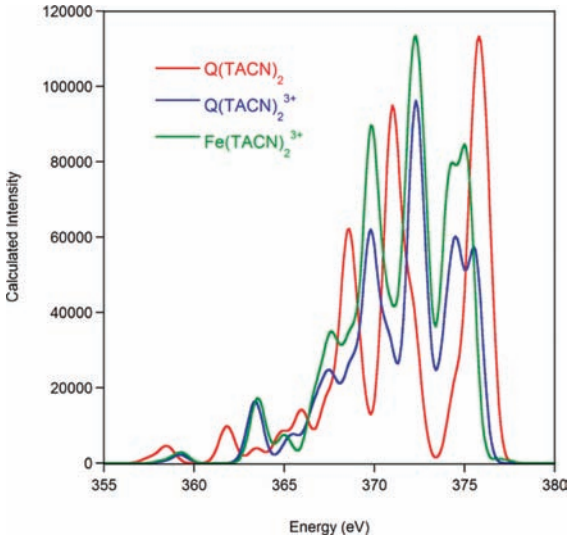

Figure 7. N Kα XES spectra of $Q(TACN)_2^0$, $Q(TACN)_2^{3+}$, and $Fe(TACN)_2^{3+}$ demonstrating effects similar to those seen when NH_3 was used as a ligand.

orbital participation in bonding that introduces electric dipole-allowed p−s character to these transitions (vide infra).

From the N Kα emission calculations, it is observed that introducing a point charge within a ligand framework stabilizes the ligand lone pairs without dramatically affecting intensities. A ferric ion has an effect very similar to that of a simple +3 point charge, stabilizing the lone pairs without impacting transition intensities. Analysis of calculated Fe valence-to-core Kβ emission reveals that the intensities are governed both by overlap with the metal orbitals and also by the symmetry of this overlap.

Given the ease with which $Fe(NH_3)_6^{3+}$ could be analyzed, a similar approach was taken with the more complex σ-only donor TACN. N Kα emission spectra were calculated for $Q(TACN)_2^0$, $Q(TACN)_2^{3+}$, and $Fe(TACN)_2^{3+}$, and, while the MO picture becomes more complicated, the same trends are observed that were seen with NH_3 as a ligand (Figure 7). Comparison to the Fe emission spectrum again shows intensity modulation by overlap between metal and ligand orbitals and by the symmetry of TACN molecular orbitals (see the Supporting Information).

While both of these examples are insightful and help to better understand XES spectra, they both involve only simple σ-donors and do not explain all observed features of the spectra, such as the split sometimes observed in the $K\beta_{2,5}$ feature when π-accepting or donating ligands are present. To delve deeper into the mechanisms governing the spectra, a complex with π-accepting ligands, $Fe(CN)_6^{3-}$, was also studied. An MO diagram and assigned N Kα emission spectrum of CN^- are shown in Figure 8.

Not surprisingly, employing an octahedral construct of six cyanides around a point charge similar to that used for NH_3 resulted in slight destabilization of most orbitals except for the lone pair, which was strongly stabilized (see the Supporting Information). The interesting contribution to the Fe XES spectrum is seen when it is overlaid with the N emission spectrum; the dominant contributions to the $K\beta_{2,5}$ region come from the cyanide σ^*_{2s-2s} and σ_{2p-2p} orbitals (Figure 9). Moreover, there is no significant contribution from the cyanide π system, presumably because the filled π orbitals of CN^- are localized between the carbon and nitrogen and have poor overlap with the metal.

dx.doi.org/10.1021/ja200560z |J. Am. Chem. Soc. 2011, 133, 5594–5601

As can clearly be seen from the molecular orbital plots A−D in Figure 9, intensity again derives from orbitals of t_{1u} symmetry.

$Fe(acac)_3$ is the only remaining compound from this series that requires analysis. The electronic complexity of the acac ligand obscures the clear-cut assignments used above, although the same general trends are apparent and are given in the Supporting Information.

Throughout this investigation, it has been seen that only transitions from molecular orbitals of t_{1u} symmetry show appreciable intensity in calculated Fe Kβ XES spectra. In octahedral symmetry, the metal p orbitals also transform as t_{1u}, allowing them to interact with any ligand-based orbitals with the same symmetry. It is this metal p contribution that imparts electric dipole-allowed character to MOs of t_{1u} symmetry, providing a mechanism for intensity not present for MOs of other symmetries. Furthermore, the interaction with metal p orbitals is mediated by distance as well, explaining the higher intensity typically seen for low spin complexes over high spin ones.

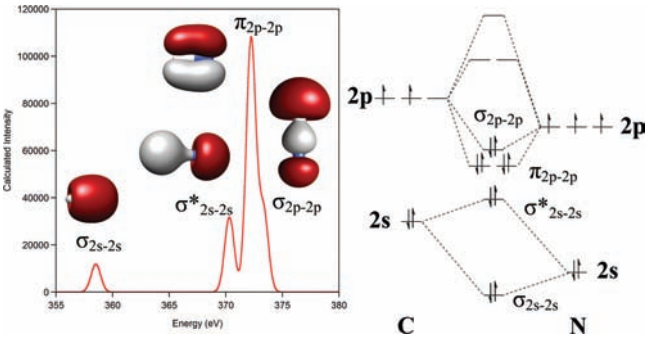

Figure 8. Molecular orbital diagram and N XES spectrum of CN^-.

Metal p Contributions to Bonding. To quantify the extent of metal p contributions to bonding, a correlation was sought between the amount of metal p character in a molecular orbital and the intensity of the corresponding XES transition signal. For all four compounds studied here, the oscillator strength of all transitions, a sum of electric dipole, magnetic dipole, and quadrupole contributions, was plotted against the amount of metal p character from each transition (Figure 10). The strong correlation obtained suggests that metal p character mixed into these orbitals provides the mechanism for intensity, as has been previously suggested.[16,32,33] No correlation was found between oscillator strength and metal s, ligand s, or ligand p character, and no stronger correlation was seen when only electric dipole moments were considered (see the Supporting Information). Additionally, the quadrupole contribution to the spectra was negligible, comprising less than 3% of observed intensity, similar to what has been observed previously.[16]

With p-character established as contributing to intensity, the next question became the origin of this p contribution: is it from metal 3p or 4p orbitals? Previous attempts to determine the nature of the metal np mixing employed the atomic natural orbital basis set ano-pVDZ and showed that both 3p and 4p contributions to the valence-to-core spectra were present.[16] This study indicated that, on one hand, Fe 3p character is borrowed from the Kβ main line and, on the other hand, 4p character may contribute to bonding. Here, we take a slightly different approach and instead ask if there is there any evidence for 4p contributions to the filled bonding orbitals.

From the output of the DFT calculations considered here, the total Fe p contribution to filled orbitals was calculated for each of

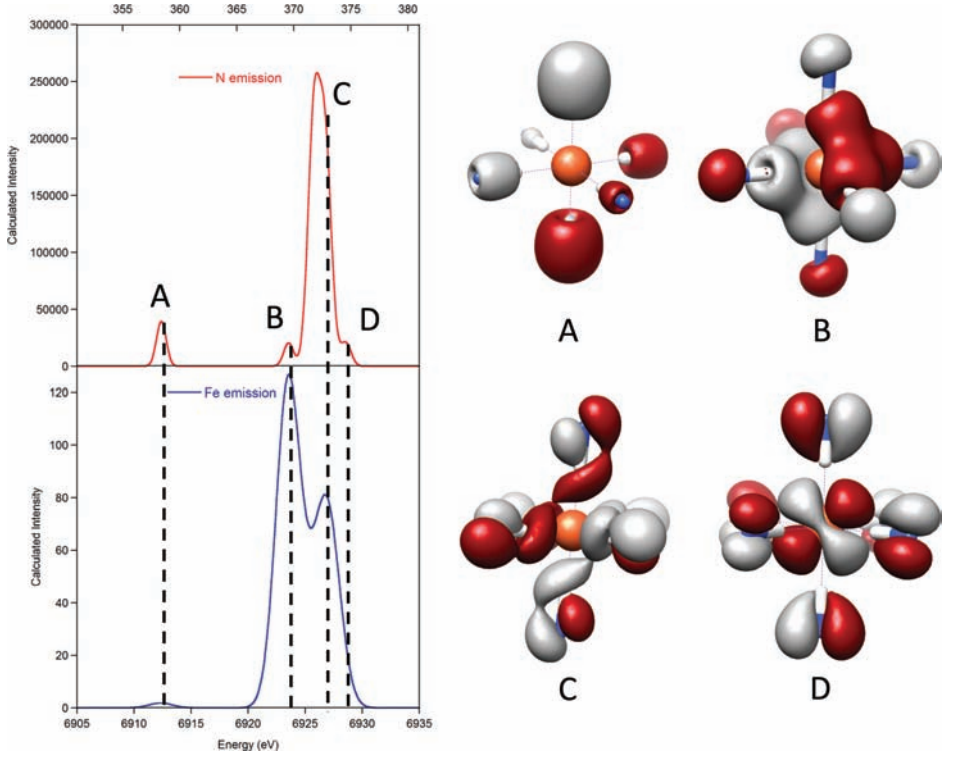

Figure 9. Correlation between Fe and N emission spectra of $Fe(CN)_6^{3-}$ showing the origin of features in Fe spectrum. The split K$\beta_{2,5}$ peak results from σ interactions between the metal and the σ^*_{2s-2s} and σ_{2p-2p} orbitals on the cyanide ligands (as seen from representative MOs B and C, respectively, plotted on the right). No significant contribution from the π system is observed.

dx.doi.org/10.1021/ja200560z |J. Am. Chem. Soc. 2011, 133, 5594–5601

the four complexes studied (Table 1). In all cases, the total Fe p character exceeded the 1200% expected for completely filled 2p and 3p orbitals (300% for each spin up and spin down electrons in both 2p and 3p), necessitating the invocation of 4p contributions to the filled MOs. The 4p values were obtained by simply subtracting 1200% from the total p amount to account for filled 2p and 3p orbitals. Furthermore, examination of the Loewdin orbital populations revealed negligible ligand contributions to the metal 3p orbitals (<1%), confirming that the p contribution here derives from the 4p and not the 3p orbitals. This supports the notion that there is very little overlap between the metal 3p and the valence ligand orbitals.

For all compounds, the amount of p character is roughly 0.8−1.5 p electrons, although what this is worth in terms of bond strength is still uncertain. To ensure that the presence of p character beyond 1200% was not simply an artifact of the calculation, the electronic structure of a free ferric ion was performed, confirming filled 2p and 3p and empty 4p, as indicated in Table 1.

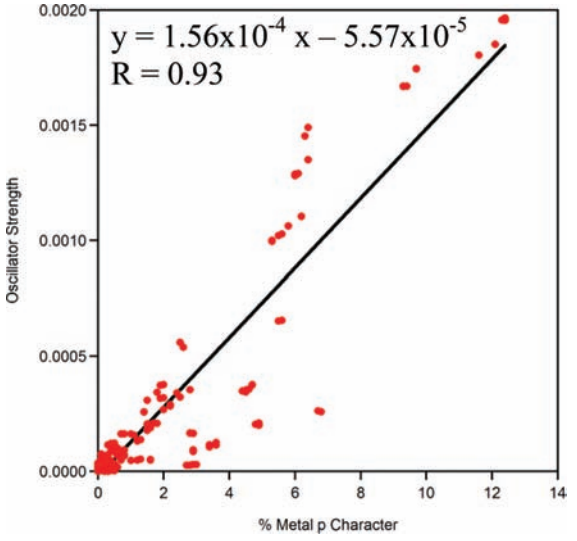

Figure 10. A strong correlation ($R = 0.93$) is seen between the amount of p character of a given transition and the oscillator strength. The small cluster of points between 2% and 7% p character that appears to fall at lower than expected intensity consists of mostly Kβ'' transitions; the reason for this low intensity is not yet understood.

Table 1. Metal 4p Character in the Compounds Studied

compound	total % p	% 4p
Fe^{3+}	1199.6%	0%
$Fe(NH_3)_6^{3+}$	1280.6%	80.6%
$Fe(CN)_6^{3-}$	1345.1%	145.1%
$Fe(TACN)_2^{3+}$	1295.5%	95.5%
$Fe(acac)_3^{3-}$	1284.4%	84.4%

DISCUSSION

The data presented herein demonstrate that valence-to-core Fe Kβ XES spectra are dominated by the electronic structure of the ligand, to the extent that the spectra can be interpreted as direct probes of the ligand molecular orbitals. These ligand orbitals are stabilized to a significant degree by the charge on the metal, thus determining the energy of the transitions seen in the XES spectrum, while the intensity is governed by the extent of Fe 4p mixing. The latter point is of particular interest as there now exists a means to experimentally quantify the extent of 4p contributions to bonding, which could lead to new insights into bonding in transition metal complexes, a topic that has been the subject of some controversy.[34−36] The contributions of both the ligand MOs and the Fe 4p interaction combine to make valence-to-core Fe XES a uniquely sensitive technique for investigating Fe coordination in complex environments.

Of particular promise for XES is its application to active site intermediates in iron-containing enzymes. In many cases, mechanistic proposals present competing pathways that are difficult to distinguish using traditional chemical methods. One such example is the extradiol dioxygenase family of enzymes that catalyze the oxidative ring cleavage of catechol derivatives. For many years, the intermediates along the reaction cycle were debated (Figure 11); specifically, it was unclear whether a side-on or end-on superoxide is formed and also whether a lactone or dioxetane intermediate is involved.[1] Recently, these questions were largely answered by a fortuitous crystal structure of one enzyme from this family,[37] although occurrences such as this are surely the exception rather than the rule. Had a crystal structure not been available, as is the case for most reactive intermediates and many other members of this enzyme family, the questions surrounding this enzyme are such that XES would likely be able to differentiate between the competing possibilities. This method thus holds promise for characterization of other members of this family of enzymes, and broadly for iron enzyme active site/substrate interactions in general.[4,5,38,39] Of particular interest is the application of XES to reactive intermediates that are not amenable to current structural characterization techniques.

For XES analysis, the two possible orientations of the superoxide should be distinguishable due to differing levels of stabilization and Fe 4p mixing for the various orbitals interacting with the metal. The side-on conformation would be expected to interact strongly through the 2p−2p π bonding orbital with a weaker interaction between the 2p−2p π^*; the end-on species, in contrast, would bond strongest through 2p−2p π^* orbitals with the 2p−2p π forming a secondary interaction. The differential stabilization of, and Fe 4p contributions to, these orbitals would

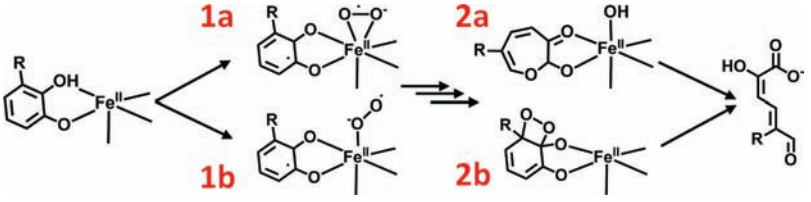

Figure 11. A condensed catalytic cycle of the extradiol dioxygenase family of enzymes showing competing proposed intermediates: a side-on superoxide (1a) versus an end-on superoxide (1b) and a lactone (2a) versus a dioxetane (2b). Figure adapted from ref1.

dx.doi.org/10.1021/ja200560z |J. Am. Chem. Soc. 2011, 133, 5594–5601

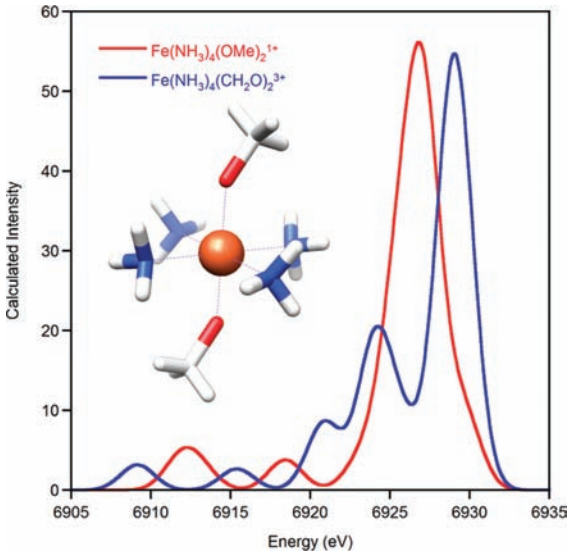

Figure 12. Calculated spectra for hypothetical $Fe^{III}(NH_3)_4X_2$ complexes, where X = $^-$OMe (red) or CH_2O (blue), to demonstrate the effect of oxygen hybridization on the XES spectra. The hypothetical $Fe(NH_3)_4(OMe)_2^+$ complex is shown with the spectra.

lead to valence-to-core XES features with characteristic energies and intensities that could be used to distinguish between the two orientations.

Similarly, the lactone and dioxetane would also possess different electronic structures and metal−ligand interactions. In the case of the dioxetane, the Fe is bound by two alkoxide oxygens, while the lactone has one alkoxide, a ketone carbonyl, and a hydroxide anion as ligands. The principal difference between these two frameworks is the presence of the carbonyl in the dioxetane; this functional group containing an sp^2 hybridized oxygen would be expected to give rise to significantly different features from the sp^3 hybridized oxygens of the dioxetane. For example, the C−O 2s−2s σ bonding orbital that can interact with the Fe would be expected to be of lower energy for the sp^2 hybridized ketone as compared to the sp^3 hybridized alkoxides, providing one means to differentiate the lactone from the dioxetane. Perhaps more significantly, the presence of the C═O would also result in significantly greater stabilization of the C−O $2p_z$−$2p_z$ σ bonding orbital, pulling this feature to lower energy as compared to the corresponding alkoxide and possibly even splitting it off from the main peak (similar to what was seen for CN^-, vide supra). Because of these effects, it is expected that XES would be able to distinguish these two intermediates as well (Figure 12).

CONCLUSIONS

A systematic computational study of the mechanisms governing valence-to-core Fe Kβ XES spectra has been presented. The features seen in these spectra derive from ligand orbitals and are dominated by two factors: stabilization due to the charge on the metal and overlap with the metal 4p orbitals. Positive charge on the metal significantly stabilizes the donor ligand orbitals to lower energy (roughly 2−3 eV for ferric ions), and thus the transitions seen in valence-to-core Fe Kβ XES are at lower energy than would be expected for the free ligands. The stabilization observed is very similar to that predicted for an unshielded +3 point charge. Intensity, meanwhile, is dictated by mixing with metal 4p orbitals, this confers dipole-allowed character to the transitions, which in turn is controlled by symmetry and orbital overlap. Only ligand orbitals possessing the appropriate symmetries are allowed to interact with the metal 4p orbitals (t_{1u} in O_h symmetry), so only these orbitals have the potential for significant intensity; orbitals that cannot mix with the metal 4p give rise to features with negligible intensity. The amount of 4p character mixed into the ligand orbitals is governed by overlap, so short bond lengths and ligand orbitals directed at the metal give rise to large intensities.

Knowing the factors behind valence-to-core XES spectra allows for better application to complicated chemical and biological systems. Because the spectra are dependent on the electronic structure, and thus complexity, of the ligands bound to the metal, this technique holds promise to elucidate catalytic intermediates, both small molecule and enzyme, during reaction cycles that would be difficult or impossible to obtain with current methods. This knowledge is also sufficiently general that it can be applied to other metals, greatly broadening the scope of valence-to-core XES spectra.

ASSOCIATED CONTENT

Supporting Information. Sample ORCA input file; calculated N emission spectra for $Q(NH_3)_6^{n+}$ (n = 0−3); comparison between N and Fe emission for $Fe(TACN)_2^{3+}$; calculated N emission for $Q(CN)_6^{n-}$ (n = 3, 6); calculated O emission for acac constructs; correlations between oscillator strength and metal s character, ligand s character, and ligand p character; and correlation between dipole-only oscillator strength and metal p character. This material is available free of charge via the Internet at http://pubs.acs.org.

AUTHOR INFORMATION

Corresponding Author
serena.debeer@cornell.edu

ACKNOWLEDGMENT

S.D. thanks Cornell University and the American Chemical Society Petroleum Research Fund (50270-DNI3) for funding.

REFERENCES

(1) Solomon, E. I.; Brunold, T. C.; Davis, M. I.; Kemsley, J. N.; Lee, S. K.; Lehnert, N.; Neese, F.; Skulan, A. J.; Yang, Y. S.; Zhou, J. *Chem. Rev.* **2000**, *100*, 235–349.

(2) Baik, M. H.; Newcomb, M.; Friesner, R. A.; Lippard, S. J. *Chem. Rev.* **2003**, *103*, 2385–2419.

(3) Costas, M.; Mehn, M. P.; Jensen, M. P.; Que, L. *Chem. Rev.* **2004**, *104*, 939–986.

(4) Hoffman, B. M.; Dean, D. R.; Seefeldt, L. C. *Acc. Chem. Res.* **2009**, *42*, 609–619.

(5) Bollinger, J. M.; Diao, Y.; Matthews, M. L.; Xing, G.; Krebs, C. *Dalton Trans.* **2009**, 905–914.

(6) Sarangi, R.; Gorelsky, S. I.; Basumallick, L.; Hwang, H. J.; Pratt, R. C.; Stack, T. D. P.; Lu, Y.; Hodgson, K. O.; Hedman, B.; Solomon, E. I. *J. Am. Chem. Soc.* **2008**, *130*, 3866–3877.

(7) Chow, M. S.; Eser, B. E.; Wilson, S. A.; Hodgson, K. O.; Hedman, B.; Fitzpatrick, P. F.; Solomon, E. I. *J. Am. Chem. Soc.* **2009**, *131*, 7685–7698.

(8) Green, M. T.; Dawson, J. H.; Gray, H. B. *Science* **2004**, *304*, 1653–1656.

(9) Westre, T. E.; Kennepohl, P.; DeWitt, J. G.; Hedman, B.; Hodgson, K. O.; Solomon, E. I. *J. Am. Chem. Soc.* **1997**, *119*, 6297–6314.
(10) Berry, J. F.; DeBeer George, S.; Neese, F. *Phys. Chem. Chem. Phys.* **2008**, *10*, 4361–4374.
(11) Funk, T.; Deb, A.; George, S. J.; Wang, H. X.; Cramer, S. P. *Coord. Chem. Rev.* **2005**, *249*, 3–30.
(12) Lee, S. K.; Nesheim, J. C.; Lipscomb, J. D. *J. Biol. Chem.* **1993**, *268*, 21569–21577.
(13) Newcomb, M.; Halgrimson, J. A.; Horner, J. H.; Wasinger, E. C.; Chen, L. X.; Sligar, S. G. *Proc. Natl. Acad. Sci. U.S.A.* **2008**, *105*, 8179–8184.
(14) Chasteen, N.; Snetsinger, P. In *Physical Methods in Bioinorganic Chemistry*; Que, L., Ed.; University Science Books: Sausalito, CA, 2000.
(15) Yang, T. C.; Maeser, N. K.; Laryukhin, M.; Lee, H. I.; Dean, D. R.; Seefeldt, L. C.; Hoffman, B. M. *J. Am. Chem. Soc.* **2005**, *127*, 12804–12805.
(16) Lee, N.; Petrenko, T.; Bergmann, U.; Neese, F.; DeBeer, S. *J. Am. Chem. Soc.* **2010**, *132*, 9715–9727.
(17) Wang, X.; Grush, M. M.; Froeschner, A. G.; Cramer, S. P. *J. Synchrotron Radiat.* **1997**, *4*, 236–242.
(18) de Groot, F. *Chem. Rev.* **2001**, *101*, 1779–1808.
(19) Glatzel, P.; Bergmann, U. *Coord. Chem. Rev.* **2005**, *249*, 65–95.
(20) Mori, R. A.; Paris, E.; Giuli, G.; Eeckhout, S. G.; Kavcic, M.; Zitnik, M.; Bucar, K.; Pettersson, L. G. M.; Glatzel, P. *Anal. Chem.* **2009**, *81*, 6516–6525.
(21) Mori, R. A.; Paris, E.; Giuli, G.; Eeckhout, S. G.; Kavcic, M.; Zitnik, M.; Bucar, K.; Pettersson, L. G. M.; Glatzel, P. *Inorg. Chem.* **2010**, *49*, 6468–6473.
(22) Neese, F.; Becker, U.; Ganyushin, D.; Hansen, A.; Liakos, D. G.; Kollmar, C.; Kossmann, S.; Petrenko, T.; Reimann, C.; Riplinger, C.; Sivalingam, K.; Valeev, E.; Wezisla, B.; Wennmohs, F. *ORCA-An Ab inito, DFT, and Semiempirical Electronic Structure Package, Version 2.7.0*; University of Bonn: Germany, 2009.
(23) Becke, A. D. *Phys. Rev. A* **1988**, *38*, 3098.
(24) Perdew, J. P. *Phys. Rev. B* **1986**, *33*, 8822.
(25) Schafer, A.; Horn, H.; Ahlrichs, R. *J. Chem. Phys.* **1992**, *97*, 2571–2577.
(26) Neese, F. *Inorg. Chim. Acta* **2002**, *337C*, 181.
(27) Klamt, A.; Schüürmann, G. *J. Chem. Soc., Perkin Trans.* **1993**, *2*, 799–805.
(28) Pettersen, E. F.; Goddard, T. D.; Huang, C. C.; Couch, G. S.; Greenblatt, D. M.; Meng, E. C.; Ferrin, T. E. *J. Comput. Chem.* **2004**, *13*, 1605–1612.
(29) Egawa, C.; Naito, S.; Tamaru, K. *Surf. Sci.* **1983**, *131*, 49–60.
(30) Rabalais, J. W.; Karlsson, L.; Werme, L. O.; Bergmark, T.; Siegbahn, K. *J. Chem. Phys.* **1973**, *58*, 3370–3372.
(31) Locht, R.; Hottmann, K.; Hagenow, G.; Denzer, W.; Baumgartel, H. *Chem. Phys. Lett.* **1992**, *190*, 124–129.
(32) Bergmann, U.; Horne, C. R.; Collins, T. J.; Workman, J. M.; Cramer, S. P. *Chem. Phys. Lett.* **1999**, *302*, 119–124.
(33) Jones, J. B.; Urch, D. S. *J. Chem. Soc., Dalton Trans.* **1975**, 1885.
(34) Landis, C. R.; Cleveland, T.; Firman, T. K. *J. Am. Chem. Soc.* **1998**, *120*, 2641–2649.
(35) Maseras, F.; Morokuma, K. *Chem. Phys. Lett.* **1992**, *195*, 500–504.
(36) Landis, C. R.; Firman, T. K.; Root, D. M.; Cleveland, T. *J. Am. Chem. Soc.* **1998**, *120*, 1842–1854.
(37) Kovaleva, E. G.; Lipscomb, J. D. *Science* **2007**, *316*, 453–457.
(38) Tinberg, C. E.; Lippard, S. J. *Biochemistry* **2009**, *48*, 12145–12158.
(39) Chen, H.; Ikeda-Saito, M.; Shaik, S. *J. Am. Chem. Soc.* **2008**, *130*, 14778–14790.